Rare Metal Materials and Engineering
Volume 53, Issue 3, March 2024
Available online at www.rmme.ac.cn

Science Press

Cite this article as: Li Yan, Li Yanbiao, Liu Qi, et al. Development and Numerical Simulation on Heat Source of K-TIG Deep Penetration Welding for Titanium Alloy[J]. Rare Metal Materials and Engineering, 2024, 53(03): 692-700. DOI: 10.12442/j.issn.1002-185X.20230320.

ARTICLE

Development and Numerical Simulation on Heat Source of K-TIG Deep Penetration Welding for Titanium Alloy

Li Yan[1,2], Li Yanbiao[1], Liu Qi[1], Yang Bingbing[2], Zhang Luxia[1], Wu Zhisheng[1]

[1] School of Materials Science and Engineering, Taiyuan University of Science and Technology, Taiyuan 030024, China; [2] School of Intelligent Manufacturing Industry, Shanxi Institute of Electronic Science and Technology, Linfen 041000, China

Abstract: K-TIG is a welding process based on traditional TIG welding, which increases the welding current to 300 A or even higher value and forms the "keyhole" effect by the feat of tungsten electrode cooling system to achieve the ultimate deep penetration welding. The welding width of K-TIG welding is wider than that of plasma and laser weld, and the weld pool is larger. The traditional heat source model is not suitable for the characteristics of heat source distribution in K-TIG weld. Based on the SYSWELD simulation platform and the experimental results of K-TIG welding for titanium alloy, a combined heat source model for numerical simulation of K-TIG deep penetration welding of titanium alloy was developed. The results show that when the distribution coefficient of double ellipsoidal heat source is 0.75 and the acting depth is 4 mm, the simulation weld pool is consistent with the actual joint cross section, and the front weld width is 12 mm and the back weld width is 5 mm. The finite element simulation results of temperature loop curve and residual stress are basically consistent with the experimental results, verifying the accuracy of the established K-TIG heat source model.

Key words: titanium alloy; K-TIG; numerical simulation; heat source development; combined heat source

As an indispensable material, medium-thick plate has been widely used in manufacturing industries such as pressure vessels, rail transportation and shipbuilding. Welding efficiency directly affects the construction cycle and cost of the product, and there is an urgent need to promote the application of efficient, high-quality, low-cost medium-thick plate welding methods. The Australian government ' s Federal Scientific and Industrial Research Organization[1] in 2000 for the first time reported K-TIG welding technology, which is based on the traditional TIG welding with welding current up to 300 A or even higher values using tungsten cooling system to form a "keyhole" effect, and ultimately achieved a large depth of melt welding method. Lathabai et al[2] compared K-TIG with conventional TIG welding for pure titanium. K-TIG is a cost-effective and highly-efficient welding method for pure titanium with a thickness of 12.7 mm under the condition of I-bevel and without filler wire, which can be successfully conducted on both sides without filler wire and beveling with stable welding process, excellent weld quality and good microstructure and mechanical properties of the weld compared with conventional TIG welding. Liu et al[3–4] used high-speed photography technology to observe "keyhole" dynamic behavior in K-TIG welding, and found that "keyhole" in K-TIG welding is clearly different from that in plasma welding, laser welding and other small-hole welding techniques. The arc is compressed in plasma welding, making the welding energy density increase significantly, while in laser welding process, due to the high energy density characteristics of the laser itself, it is able to obtain a stable small hole with small melt width and large melt depth. But K-TIG welding arc increases the arc energy density by increasing the current, arcs only form after the shielding gas compression; for ordinary arc, the macro-state weld melt width is wider compared with that of plasma welding, laser welding and other welding methods, and the melt pool volume is large[5].

Received date: May 28, 2023
Foundation item: Key R&D Program of Shanxi Province (202102050201001); Shanxi Basic Research Plan (202203021221149); Linfen Key Research and Development Plan (2202)
Corresponding author: Li Yan, Ph. D., Associate Professor, School of Materials Science and Engineering, Taiyuan University of Science and Technology, Taiyuan 030024, P. R. China, E-mail: yanli1988@tyust.edu.cn

The above research is mainly from the experimental point of view for K-TIG welding seam forming laws and welding "keyhole" mechanism, but numerical simulation for K-TIG welding is seldom reported. With the development of computer technology, numerical simulation is increasingly used in welding-related research to avoid the cost of multiple experiments, and there is a variety of analytical tasks to complete the experiment[6]. Accurate simulation of the actual welding process has become the direction for researches, and the most important thing is the accurate description of the welding heat source model[7–8]. The accuracy of the heat source model directly affects the accuracy of the simulation results[9]. Due to the small hole characteristics of K-TIG deep melt welding, traditional TIG heat source model is no longer applicable. The combined heat source model can better adapt to various melt pool shapes and reflect the characteristics of the distribution of welding heat in the depth direction in the medium-thick plate welding simulation, and thus it is widely used[10–11]. To expand the application of K-TIG welding technology, based on SYSWELD simulation platform and titanium alloy K-TIG welding experimental results, we studied the development of titanium alloy K-TIG deep melt welding simulation with combined heat source model, and analyzed the temperature field in welding process and stress distribution law. The results of the study can provide theoretical reference for large titanium alloy K-TIG welding deformation and stress prediction.

1 Experiment

The test material was TC4 titanium alloy with the dimensions of 350 mm×150 mm×8 mm, and Ao Tai ATIG-1000 welding power was used for welding experiments. K-TIG priming welding had no wire filling, no opening of the breach and no gap. Welding process parameters are shown in Table 1.

When the welding test was conducted, a K-type thermocouple was buried on the upper surface of the test plate, and the HP-8125 dynamic data acquisition system was connected to the thermocouple to collect the thermal cycling curve of the thermocouple position during the welding process. At the same time, the Sigmar-ASM blind hole method of stress measurement instrument was used to measure the residual stress at some key points on the upper surface of the welded specimen, including transverse residual stress (residual stress perpendicular to the welding direction) and longitudinal residual stress (residual stress parallel to the welding direction). The principles of the blind hole method used to measure weld residual stresses were described in Ref. [12]. Hollow dots in Fig. 1 indicate the location of the buried thermocouple, and solid dots indicate the location of the residual stress perforation.

Fig. 2 shows the completion of the welding for titanium alloy test plate. The weld surface is bright yellowish, the front and back of the weld are well formed, and the back of the weld penetration indicates that the welding process forms a stable welding "keyhole", suggesting the successful realization of single-sided welding and double-sided molding. The wire cutting machine tools were used to prepare metallographic specimens of K-TIG welding joint. Fig. 3 shows the macroscopic shape of the joint after K-TIG priming welding. It can be seen that K-TIG welding is similar to laser

Table 1 Welding process parameters of K-TIG

Welding current, *I*/A	Welding voltage, *U*/V	Welding speed/mm·min^{-1}	Protective gas	Protective gas flow/L·min^{-1}
450	17	380	99.99% Ar	30

welding, plasma welding and other small-hole type welding methods, as a one-time penetration technology, and the melt pool presents a wide "funnel-shaped". As the K-TIG welding arc is not compressed, the front of the weld is wider. K-TIG welding process is not filled with wire because of the base material self-melting. The role of surface tension leads to the welding in the middle of high and low sides, and the biting defect appears.

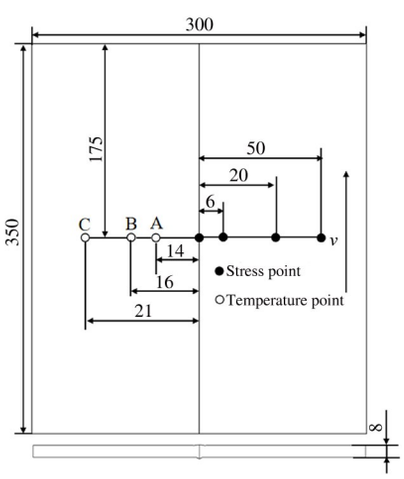

Fig.1 Test point location diagram

2 Simulation

2.1 Finite element model

According to the size of the welded test plate and the macroscopic metallographic dimensions of the joint in Fig. 3, the simulation geometry model is established, as shown in Fig. 4. A gradient hexahedral mesh is used to discretize the model, the weld zone and the heat-affected zone of the mesh are fine, and the area away from the weld base material adopts sparse mesh division. The simulation model has a total of 69 650 3D cells and 80 608 nodes, of which the minimum cell length is 0.5 mm.

Considering the nonlinear characteristics of the material

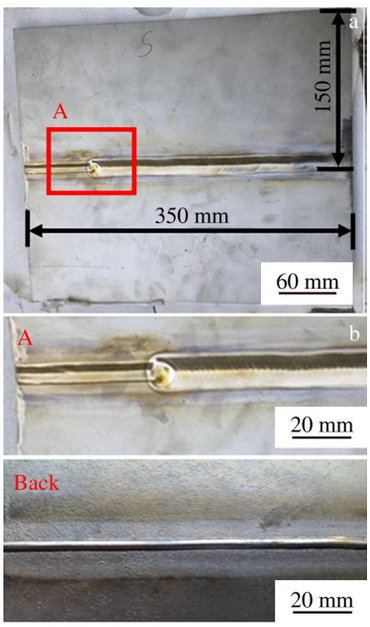

Fig.2 Titanium alloy welded plate

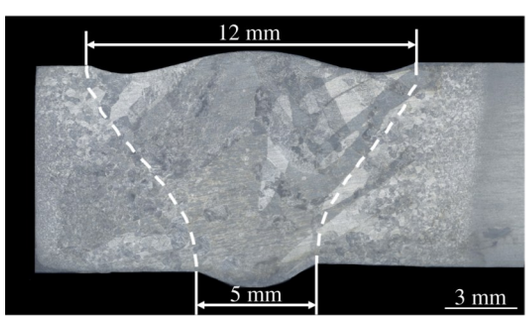

Fig.3 Macroscopic topography of the joint

properties in the welding process, JMatPro was used to calculate the thermophysical and thermomechanical parameters of TC4, as shown in Fig.5.

2.2 Welding heat source model

K-TIG welding is a typical small-hole welding process. Among the existing small-hole welding methods, plasma arc welding is also developed based on traditional TIG welding by contracting the arc and increasing the energy density of the arc, which is highly similar to K-TIG welding. Hu et al[13] used a combined heat source in the form of a double ellipsoidal heat source in the upper half and a cylindrical heat source in the lower half to obtain simulation results for plasma welding that closely match the actual situation; the double ellipsoidal model in the combined heat source approximates the ablation of the material by the arc, as well as the arc pressure effect in a wide range; the cylindrical heat source model simulates the effect of the longitudinal direction in the central region after the formation of small holes. Therefore, in the present K-TIG welding simulation, we also selected the double ellipsoidal heat source in the upper half and the cylindrical heat source in the lower half, i. e., a combined heat source, and the heat source model schematic is shown in Fig.6.

As for double ellipsoidal heat source function[14], the first half ellipsoid can be expressed as:

$$Q_{\mathrm{f}}(x,y,z)=\frac{6\sqrt{3}\left(f_{\mathrm{f}}Q\right)}{a_{\mathrm{f}}bc\pi\sqrt{\pi}}\exp\left(-\frac{3x^2}{a_{\mathrm{f}}^2}-\frac{3y^2}{b^2}-\frac{3z^2}{c^2}\right)\quad x>0 \quad (1)$$

The posterior semi-ellipsoid can be expressed as:

$$Q_{\mathrm{r}}(x,y,z)=\frac{6\sqrt{3}\left(f_{\mathrm{f}}Q\right)}{a_{\mathrm{r}}bc\pi\sqrt{\pi}}\exp\left(-\frac{3x^2}{a_{\mathrm{r}}^2}-\frac{3y^2}{b^2}-\frac{3z^2}{c^2}\right)\quad x\leqslant 0 \quad (2)$$

$Q_{\mathrm{f}}(x, y, z)$ is the heat flow distribution in the volume of the front hemisphere; $Q_{\mathrm{r}}(x, y, z)$ is the heat flow distribution in the volume of the posterior hemisphere; a_1, a_2, b and c are the shape parameters of the double ellipsoid model, as shown in Fig. 6a. Since the actual effective range of the arc cannot be measured directly, Goldak suggested to use the macroscopic shape dimensions of the weld cross-section as the initial shape parameters of the model, and b and c were taken as the actual melt pool half-width and the actual melt depth, respectively, who specified the first 1/4 ball length a_{f} as half of the melt width and the second 1/4 ball length a_{r} as twice of the melt width.

The cylindrical heat source function is follows:

$$q(r,0)=\frac{3Q_2x}{\pi R^2h}\exp\left(\frac{-3r^2}{R^2}\right) \quad (3)$$

Gaussian column heat source model sets the radial heat flow of the column heat source as Gaussian distribution, while uniform distribution in the depth direction of the column, and the heat source is an embedded cylinder. h is the welding melt depth and R is the radius of action of the heat source, as shown in Fig.6b.

In the combined heat sources for welding simulation, the double ellipsoidal heat source load action height is defined as

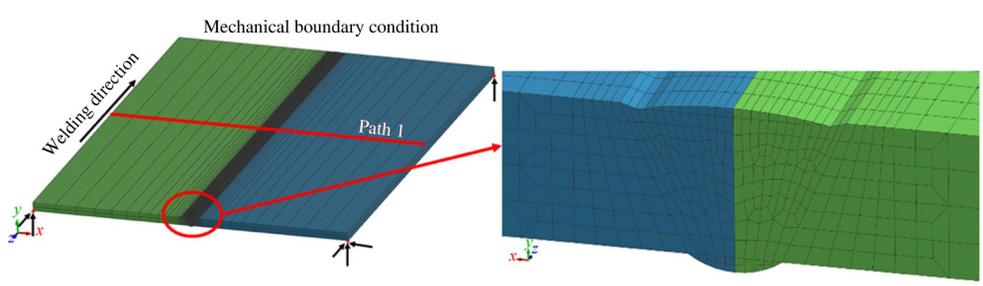

Fig.4 Finite element model of plate butt joint

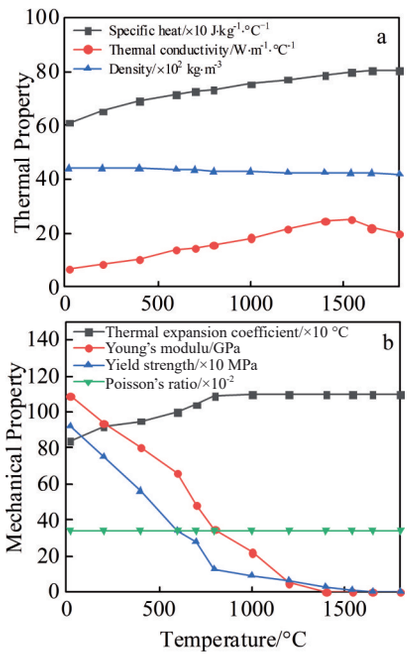

Fig.5 Thermal properties (a) and mechanical properties (b) of TC4 material

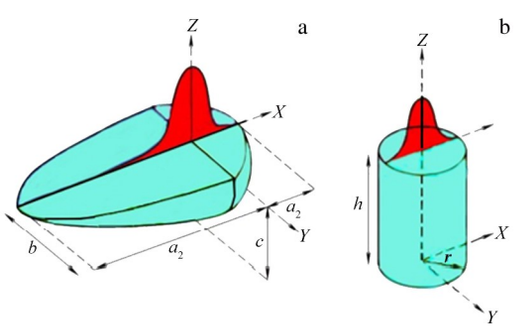

Fig.6 Schematic diagrams of heat source model: (a) double ellipsoidal heat source and (b) cylinder heat source

H, Gaussian cylinder heat source load action height is defined as h, single-pass welding melt depth is defined as Z, and $Z=H+h$. The proportion coefficient of each combined part of the heat source power accounts for the total heat source power, known as the power distribution coefficient. Double ellipsoidal heat source distribution coefficient is X_d, and Gaussian cylinder heat source distribution coefficient is X_c, satisfying $X_d+X_c=1$ and $Q_d+Q_c=Q_{effective}$. K-TIG deep fusion welding total power $Q_{effective}=\eta UI$, where η is the effective coefficient. Since larger part of the arc heat production in the K-TIG welding process is used to vaporize the metal to produce small holes, the energy utilization rate is relatively low, the effective coefficient η in the simulation is taken as 0.55[15], and in this welding experiment $Q_{effective}=\eta UI=0.55\times17\times450=4207.5$ W.

According to macroscopic metallographic dimensions of welded joints in Fig.3, the initial parameters of the simulation are determined, as shown in Table 2.

When using the combination of heat source simulation, the depth of action of the heat source and the heat source distribution coefficient have a significant impact on the simulation results, and unreasonable values will make the role of one of the heat source to be masked by the other heat source. According to the welding simulation pool boundary guidelines, the depth of action of the heat source and the energy distribution coefficient are obtained through the simulation and experimental cross-checking, and the calibration scheme is shown in Table 3.

The controlling equation for the heat transfer of the arc heat in the workpiece during welding is as follows.

$$\lambda\left(\frac{\partial^2 T}{\partial x^2}\right)+\lambda\left(\frac{\partial^2 T}{\partial y^2}\right)+\lambda\left(\frac{\partial^2 T}{\partial z^2}\right)+q_v=\rho c\frac{\partial T}{\partial t} \quad (4)$$

where T is the temperature; λ is the heat conduction coefficient; q_v is the heat generating power of the internal heat source; ρ is the density; c is the specific heat capacity; t is the heat transfer time; x, y and z are the coordinates in the plenary coordinate system (x, y, z).

The workpiece not only absorbs heat from the arc and molten metal droplets during the welding process, but also dissipates heat to the surrounding environment, so the heat exchange between the workpiece and the external environment is considered in the finite element model by defining the heat dissipation surface. This study considers two forms of heat loss, i. e., convection and radiation heat loss, through Newton's law and Stefan-Boltzmann's law[16].

3 Heat Source Calibration

Based on the thermal-elastic-plastic finite element method, the simulation calculation results of temperature field which is the same as that of the actual welding process are obtained. Using the welding simulation melt pool boundary guidelines for heat source calibration, simulated melt pool size and the actual welded joint cross-section melt pool size are compared, and if the simulated melt pool area boundary and the actual welding melt pool size match, it can be considered that the selected heat source model is reasonable[17–18].

Fig. 7 shows the shape of the melt pool along the welding direction of the central cross-section, and the temperature field post-processing will be higher than the titanium alloy melting point (1650 °C) temperature area set as gray for the melt pool region. The region with a peak temperature between 650 and 1650 °C is the heat-affected zone. Fig. 7a is the simulation temperature field cloud of Scheme 1, with X_d=0.65 and H=2 mm as combination of heat source parameters, and the

Table 2 Initial geometric parameters of the heat source for K-TIG

Heat source	a_f/mm	a_r/mm	b/mm	c/mm	R/mm
Double ellipsoidal+cylindrical	3.4	6.6	12	2	2.5

Table 3 Heat source parameter calibration scheme

Scheme	Upper double ellipsoidal heat source		Lower Gaussian cylinder heat source	
	X_d	H/mm	X_c	h/mm
1	0.65	2	0.35	6
2	0.65	4	0.35	4
3	0.65	6	0.35	2
4	0.75	2	0.25	6
5	0.75	4	0.25	4
6	0.75	6	0.25	2
7	0.85	2	0.15	6
8	0.85	4	0.15	4
9	0.85	6	0.15	2

workpiece is fully melted through the formation of root holes. The simulation of the melt pool shape shows the width of the "funnel shape", and is basically consistent with the actual welded joint cross-sectional shape, which has slightly larger front melt width of 13.5 mm and slightly smaller back melt width of 4 mm. Fig. 7b is the simulated temperature field cloud chart of Scheme 2, with X_d=0.65 and H=4 mm as combination of heat source parameters. Compared with Scheme 1, the frontal melt width becomes narrower, and the back melt width becomes larger. This is due to the increase in depth of action of the double ellipsoidal heat source. The double ellipsoidal heat source energy in the root of the weld is not concentrated, the back of the weld width increases in the welding process, the size of the "keyhole" becomes larger, and the melt pool volume increases. At this time, the surface tension of the liquid melt pool has been unable to hold the melt pool of liquid metal, which in turn will cause the actual welding of the melt pool. Lathabai et al[19] pointed out that the liquid melt pool must be held by the surface tension under a condition that it must be met to achieve a stable "keyhole" weld, and introduce an inequality between the root channel width w, plate thickness h, surface tension γ and density ρ: $wh<\lambda/\rho g$. It shows that under certain conditions, the narrower the back side weld channel, the more stable the small hole. Fig.7c is the simulated temperature field cloud of Scheme 3, with X_d= 0.65 and H=6 mm as combined heat source parameters, in which the melt pool is transformed from "funnel-shaped" to "trapezoidal", and the actual welded joint cross-sectional shape shows a large difference. Comprehensive results of Schemes 1–3 simulation can be seen in the case of constant heat distribution coefficient. As the double ellipsoidal heat source depth of action increases, the melt width of melt pool upper surface decreases, and the back melt width will increase, which is not conducive to the formation of "keyhole", so the actual welding will produce welding collapse, and cannot produce the effect of single-sided welding+double-sided molding.

According to the above nine groups of tests, it is known that a combined heat source model with a double ellipsoidal heat source distribution coefficient of 0.75 and a double ellipsoidal heat source action depth of 4 mm should be selected for the numerical simulation of K-TIG deep fusion welding of 8 mm titanium alloy. With these parameter, the dimensions of the simulated weld zone and heat affected zone match well with the actual joint, as shown in Fig. 8, which proves the reasonableness of the heat source model.

4 Simulation Model Selection

4.1 Temperature field analysis

By solving the established model, the transient temperature field distribution of the test plate in welding process is shown in Fig. 8. Fig. 8a, 8c and 8e show the transient temperature field distributions of upper surface of workpiece after the start of welding at 5, 25 and 50 s, respectively. The melt pool of upper surface is in ellipsoidal shape, and as the welding progresses, the melt pool continues to move. In front of the heat source, isotherm is dense, the temperature gradient is large, while behind the heat source, the isotherm is sparse, and the temperature gradient is small. The temperature field distribution remains consistent with double ellipsoidal heat source mathematical model. Fig.8b, 8d and 8f show transient temper-

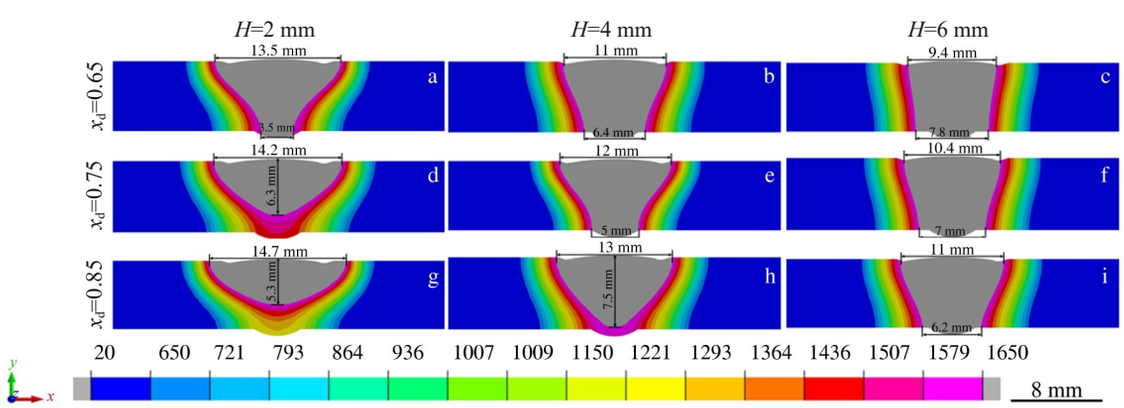

Fig.7 Comparison of heat source parameters and melt pool size under different conditions

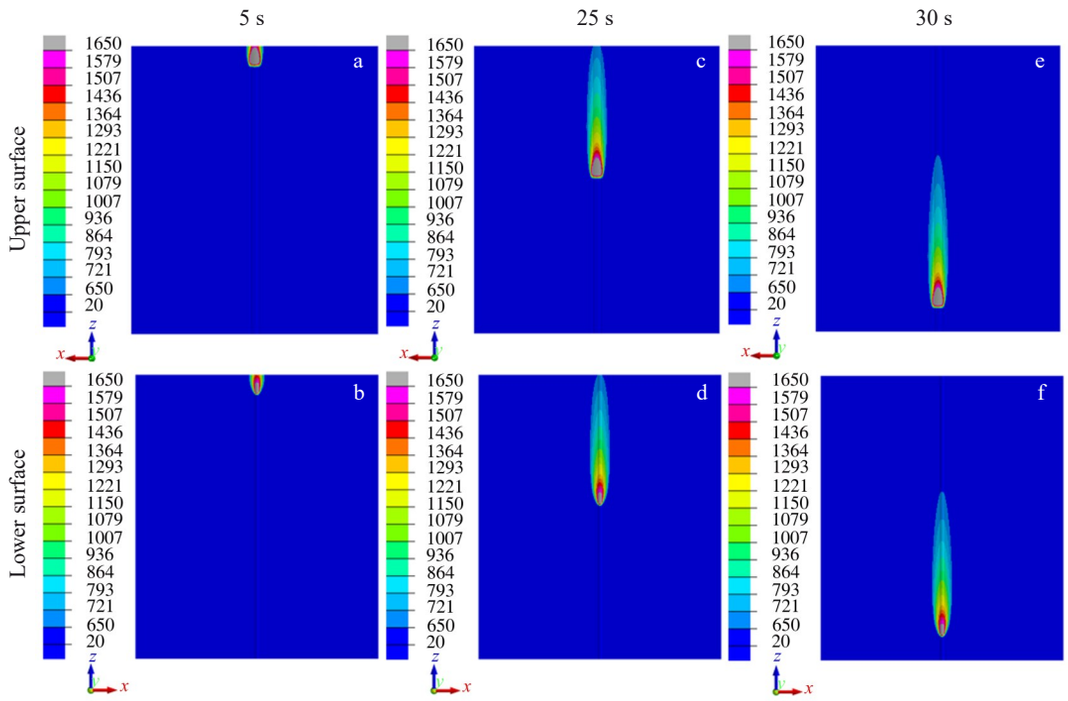

Fig.8 Temperature field distribution of upper (a, c, e) and lower (b, d, f) surfaces of workpiece in K-TIG welding at different time: (a–b) 5 s, (c–d) 25 s, and (e–f) 50 s

ature field distributions of the lower surface at corresponding moments. The lower surface melt pool size is small, and a stable moving "keyhole" will form in the actual welding.

In the experiments, the thermal cycle curves at three locations (8, 10 and 15 mm from the weld toe) are recorded by K-type thermocouples. For comparison, the corresponding thermal cycle data from the numerical model of these three locations (point A, point B and point C in Fig. 1) were also extracted, and the calculated and experimental results are shown in Fig. 9. It can be seen that although there are some local differences between the calculated value and the experimental value, the predicted peak temperature and temperature rate at each point are in good agreement with the

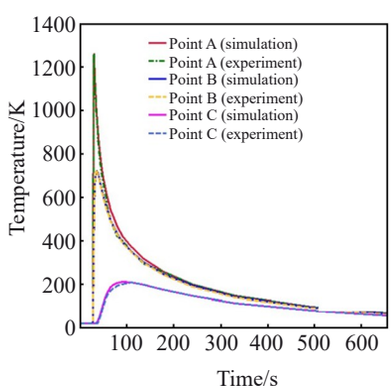

Fig.9 Comparison between simulation results and experimental results of welding thermal cycle

experimental results, but there are some differences between the cooling rate and the measured curve, due to the differences in simulated thermal property, boundary conditions and the actual welding[20]. The processing hardening layer of TC4 titanium alloy is not significant and the effect of phase change on the residual stress generation is less, so such differences in the welding cooling rate are within an acceptable range[21–22]. The comparison of the melt pool morphology and temperature cycling curves shows that the finite element model established in this study and the used heat source model can accurately restore the heat input during the actual welding process.

4.2 Stress field analysis

The results of the temperature field calculation as a thermal load are loaded into the thermal-elastic-plastic finite element module for welding stress calculations. Fig. 10 shows transverse and longitudinal stress distributions after the K-TIG welding followed by cooling to 100 ° C. In the direction parallel to the weld, there is a stress stability region in the middle position of the welded plate, while the stress at the head and tail ends of the weld is less, which is due to the free ends of the weld, resulting in less constraint during the cooling and shrinkage of the weld. In the direction perpendicular to the weld, the weld and heat-affected zone produce a large longitudinal and transverse residual tensile stress locally after heating and cooling, due to the constraint by surrounding lower-temperature metal, while a large compressive stress is formed in the heat-affected zone on both sides because of the stress balance.

In the central cross-sectional position perpendicular to the welding direction, set path 1 (Fig.4) to observe transverse and

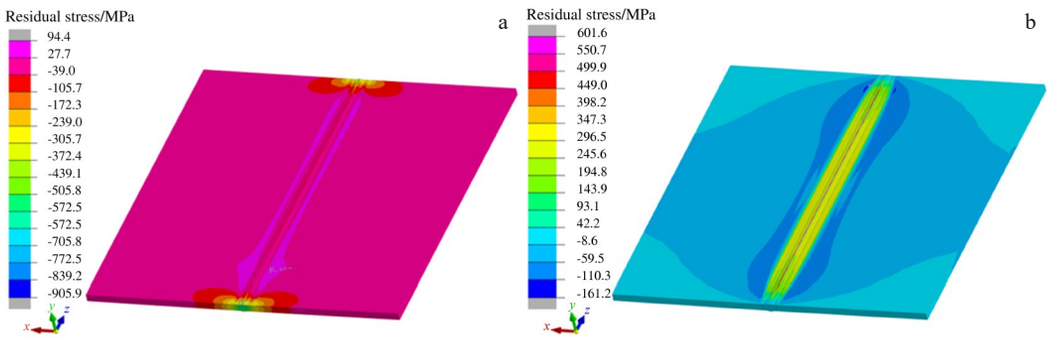

Fig.10 Nephogram of transverse (a) and longitudinal (b) residual stress distributions on the surface of the test plate

longitudinal stress distribution clouds after K-TIG welding, as shown in Fig. 11. Weld and heat-affected zone at the resulting stress concentration area along the centerline of the weld show a symmetrical stress distribution. The transverse residual stress distribution in central section ranges from −905.9 MPa to 94.4 MPa, and longitudinal residual stress ranges from −161.2 MPa to 601.6 MPa, which are much smaller than the material yield limit at room temperature (942 MPa)[23], thereby indicating that although the weld and its adjacent areas produce large plastic deformation, the degree of titanium alloy TC4 work hardening is not significant, so the post-weld residual stress in this area will be lower than the yield strength of the parent material[24–25]. In addition, the transverse tensile stress of the joint is much lower than the longitudinal tensile stress, mainly because the welding test is done under the condition of no external constraint, so the joint is subjected to a smaller transverse constraint than the longitudinal constraint[26–27]. Besides, significant transverse stress concentrations appear on the upper surface of the weld and at the root of the weld, mainly due to changes in the geometry of the joint at the weld toe area. The transverse and longitudinal stresses in the central section are high tensile stresses in the weld zone and heat-affected zone of the joint and compressive stresses away from these regions.

Fig. 12 shows the simulation results and blind hole method measurements of the transverse and longitudinal stresses on the upper surface of path 1 test plate. The surface stress distribution in path 1 is consistent with the cross-sectional stress characteristic cloud in Fig. 12. Transverse stress in the middle region of the weld is subjected to compressive stress, and in the weld toe and heat-affected zone location, it has higher values of tensile stress, with the peak stress of 94.4

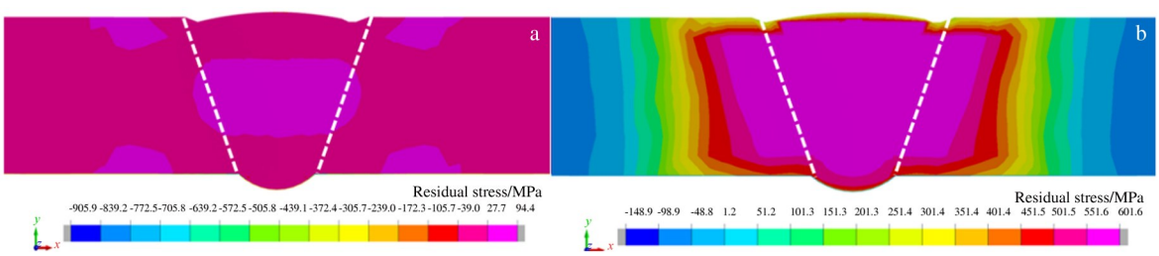

Fig.11 Transverse (a) and longitudinal (b) residual stress distributions at the center section in the welding direction

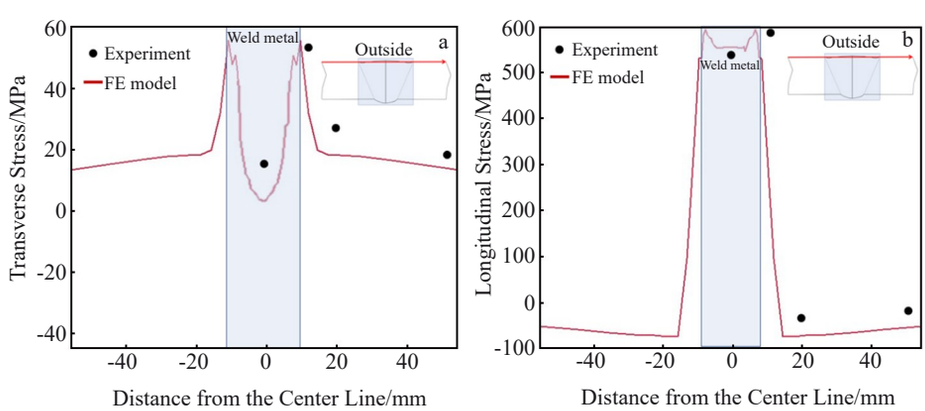

Fig.12 Transverse (a) and longitudinal (b) residual stress distributions in path 1

MPa. The hump is located at the toe of the weld, with a peak stress of 601.6 MPa, which is due to the strong confinement of the weld metal during cooling by the relatively low temperature of the surrounding material. The upper surface of path 1 away from the weld area is in a low stress state. Comparing the simulation results with the experimental results by blind hole method, there are some differences in the stress values near the weld and heat-affected zone, but the trends of stress changes reflected by both simulation results and experiments are basically consistent. Compared with that of the longitudinal stress, the measurement error of transverse stress is greater because the generation of transverse stress is indirectly affected by the longitudinal shrinkage of the weld metal in addition to the transverse shrinkage of the weld, and usually, it is difficult to obtain accurate measurements of transverse stress[28]. In the location away from the weld, there is a difference of about 50 MPa between the calculated and experimental values, and the experimental values measured by the blind hole method are greater than the numerical simulation values, mainly because the initial residual stress exists in the test plate before welding, and the welding heat input has little effect on the initial residual stress in the area away from the weld[29–30]. Simulation and experimental test stress results show that the heat source model developed in this study can effectively and accurately assess the stress distribution in deep-fusion welding.

5 Conclusions

1) Based on the temperature field simulation of the fusion line criterion, in the numerical simulation of K-TIG deep fusion welding for 8 mm titanium alloy, a combination of heat sources is used, with double ellipsoidal heat source distribution coefficient of 0.75 and the depth of action taken as 4 mm. The simulation of the melt pool and the actual cross-section of the joint match well, with the frontal fusion width of 12 mm and back fusion width of 5 mm.

2) Comparison of temperature thermal cycling curve results shows that the finite element model established in this study and the use of heat source model can accurately restore the actual heat input during the welding process.

3) The residual stresses obtained by thermal-elastic-plastic finite element calculations and test results by blind hole method are basically the same, indicating that the finite element model established in this study can effectively and accurately assess the deep-fusion welding stress distribution.

References

1 Jarvis B L. *Keyhole Gas Tungsten Arc Welding: A New Process Variant*[D]. Wollongong: University of Wollongong, 2001

2 Lathabai S, Jarvis B L, Barton K J. *Materials Science and Engineering A*[J], 2001, 299(1–2): 81

3 Liu Z M, Fang Y X, Cui S L *et al. Journal of Materials Processing Technology*[J], 2016, 238: 65

4 Liu Z M, Fang Y X, Cui S L *et al. International Journal of Thermal Sciences*[J], 2017, 114: 352

5 Jarvis B L, Ahmed N U. *Science and Technology of Welding and Joining*[J], 2000, 5(1): 1

6 Xu Zhou, Li Xiaoyan, Wang Xiaopeng *et al. Materials Reports*[J], 2022, 36(6): 152 (in Chinese)

7 Wang Xiaopeng, Li Xiaoyan, Wu Qi *et al. Materials Reports*[J], 2020, 34(10): 2008 (in Chinese)

8 Huang B S, Chen Q, Yang J *et al. Transactions of the China Welding Institution*[J], 2019, 40(2): 138

9 Wu Chuansong. *Welding Thermal Process and Molten Pool Dynamic*[M]. Beijing: Mechanical Industry Press, 2007: 16 (in Chinese)

10 Jazeel, Rahman, Chukkan *et al. Journal of Materials Processing Technology*[J], 2015, 219: 48

11 Dai W, Song Y, Xin J *et al. Fusion Engineering and Design*[J], 2020, 154: 111538

12 Deng Dean, Kiyoshima S. *Acta Metallurgica Sinica*[J], 2010, 46(2): 195 (in Chinese)

13 Hu Qingxiang. *Finite Element Analysis of Temperature Fields in Keyhole Plasma Arc Welding*[D]. Jinan: Shandong University, 2007 (in Chinese)

14 Goldak J, Chakravarti A, Bibby M. *Metallurgical Transactions B*[J], 1984, 15(2): 299

15 Huang Yifeng, Luo Zhen, Wang Zhengming *et al*. *Transactions of the China Welding Institution*[J], 2017, 38(11): 103 (in Chinese)

16 Dai Peiyuan, Hu Xing, Lu Shijie *et al. Acta Metallurgica Sinica* [J], 2019, 55(8): 1058 (in Chinese)

17 Li Ziliang, Liu Janqiao, Ren Shendong *et al. Journal of Mechanical Engineering*[J], 2018, 54(10): 59 (in Chinese)

18 Tang Qi, Chen Peng, Chen Jingqing *et al. Transactions of the China Welding Institution*[J], 2019, 40(3): 32 (in Chinese)

19 Xia Mingxing, Zheng Xin, Li Zhongkui. *Materials China*[J], 2008, 27(12): 22 (in Chinese)

20 Hu X D, Yang Y C, Song M. *Materials*[J], 2019, 12(21): 3489

21 Li Suo, Ren Sendong, Zhang Yanbin *et al. Journal of Materials Processing Technology*[J], 2017, 244: 240

22 Wu G D, Shen J F, Zhang W J *et al*. *Rare Metal Materials and Engineering*[J], 2023, 52(3): 798

23 Cong Chengming, Zeng Caiyou, Zhang Yupeng *et al*. *Hot Working Technology* [J], 2023, 13: 1 (in Chinese)

24 Hu Xing, Dai Peiyuan, Zhang Chaohua *et al. Journal of Mechanical Engineering*[J], 2019, 55(12): 72 (in Chinese)

25 Deng Dean, Kiyoshima S. *Acta Metallurgica Sinica*[J], 2014, 50(5): 626 (in Chinese)

26 Luo Y. *Description of Inherent Strain and Its Application to Prediction of Welding Deformation and Residual Stress Under Multi-pass Welding*[D]. Osaka: Osaka University, 1997

27 Li S, Ren S D, Zhang Y B *et al*. *Journal of Materials Processing*

Technology[J], 2017, 244: 240

28 Deng D A, Kiyoshima S. *Nuclear Engineering and Design*[J], 2010, 240(4): 688

29 Leggatt R H. *International Journal of Pressure Vessels & Piping*[J], 2008, 85(3): 144

30 Pu X W, Zhang C H, Li S *et al*. *The International Journal of Advanced Manufacturing Technology*[J], 2017, 93: 2215

钛合金K-TIG深熔焊热源开发与数值仿真

李　岩[1,2]，李艳彪[1]，刘　琪[1]，杨冰冰[2]，张璐霞[1]，吴志生[1]

(1. 太原科技大学 材料科学与工程学院，山西 太原 030024)

(2. 山西电子科技学院 智能制造产业学院，山西 临汾 041000)

摘　要：K-TIG是在传统TIG焊基础上，将焊接电流提高到300 A甚至更高并配合钨极冷却系统形成“匙孔”效应，最终实现大熔深的焊接工艺方法。K-TIG焊缝熔宽相对于等离子和激光焊接等焊接方法较宽，熔池体积较大。传统的热源模型不适合K-TIG焊热源分布特点，基于SYSWELD仿真平台和钛合金K-TIG焊接实验结果，开发钛合金K-TIG深熔焊数值仿真组合热源模型。结果表明，双椭球热源分配系数取0.75，作用深度取4 mm时，仿真熔池与实际接头横截面相符，正面熔宽为12 mm，且背部熔宽为5 mm。温度热循环曲线和残余应力有限元仿真结果与实验结果基本一致，验证了所建立的K-TIG热源模型的准确性。

关键词：钛合金；K-TIG；数值模拟；热源开发；组合热源

作者简介：李　岩，男，1988年生，博士，副教授，太原科技大学材料科学与工程学院，山西 太原 030024，E-mail：yanli1988@tyust.edu.cn